

A Photohormone for Light-Dependent Control of PPAR α in Live Cells

Sabine Willems,[§] Johannes Morstein,[§] Konstantin Hinnah,[§] Dirk Trauner,^{*} and Daniel Merk^{*}

Cite This: *J. Med. Chem.* 2021, 64, 10393–10402

Read Online

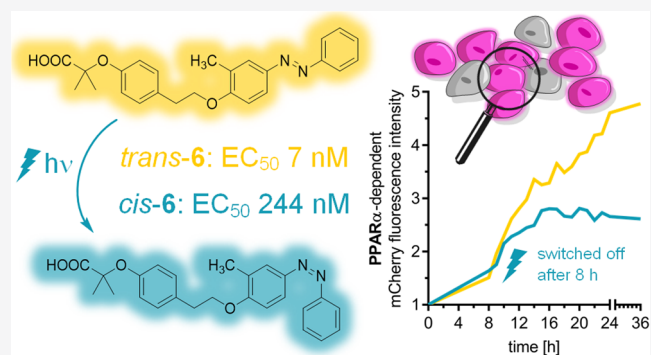
ACCESS |

Metrics & More

Article Recommendations

Supporting Information

ABSTRACT: Photopharmacology enables the optical control of several biochemical processes using small-molecule photoswitches that exhibit different bioactivities in their *cis*- and *trans*-conformations. Such tool compounds allow for high spatiotemporal control of biological signaling, and the approach also holds promise for the development of drug molecules that can be locally activated to reduce target-mediated adverse effects. Herein, we present the expansion of the photopharmacological arsenal to two new members of the peroxisome proliferator-activated receptor (PPAR) family, PPAR α and PPAR δ . We have developed a set of highly potent PPAR α and PPAR δ targeting photohormones derived from the weak pan-PPAR agonist GL479 that can be deactivated by light. The photohormone **6** selectively activated PPAR α in its *trans*-conformation with high selectivity over the related PPAR subtypes and was used in live cells to switch PPAR α activity on and off in a light- and time-dependent fashion.



INTRODUCTION

Photopharmacology utilizes photoswitchable small molecules as tools to obtain optical control of biological activity and modulate cellular processes with unprecedented spatiotemporal resolution.^{1–4} While this approach has been successfully established to control ion channels,^{5,6} membrane receptors,^{7–9} transporters,^{10–13} and enzymes,^{14–16} nuclear receptors (NRs) are fairly new to this proceeding. Upon binding of mainly amphiphilic ligands, NRs interact with specific DNA response elements to regulate the transcription of their target genes.^{17,18} The success of photoswitchable lipids¹⁹ suggests that fatty acid mimetic²⁰ NR ligands could also be suitable for photopharmacology. This could indeed be demonstrated with a few classes of NRs, including retinoic acid receptor α (RAR α), which can be optically controlled by a photoswitchable retinoic acid derivative.²¹ Subsequently, we have developed dedicated photohormones for the bile acid-activated transcription factor farnesoid X receptor (FXR)²² and the fatty acid-sensing peroxisome proliferator-activated receptor γ (PPAR γ),²³ and Tsuchiya et al. have reported a photoswitchable estrogen receptor (ER) agonist.²⁴ Still, in light of their value as chemical tools for pharmacology, the collection of available photo-switchable ligands for transcription factors is scarce.

The NRs' function governs multiple physiological processes, comprising embryonal development, cell proliferation, differentiation, metabolism, and homeostasis.²⁵ NR modulation by a wide variety of endogenous ligands, including thyroid and steroid hormones, bile acids, fatty acids, and vitamins causes intermediate (minutes) to prolonged (hours–days) actions.^{17,26}

The PPARs, belonging to the subfamily I of NRs (NR1C), comprise three isoforms PPAR α , PPAR δ , and PPAR γ , which are fatty acid- and lipid-activated transcription factors essentially involved in metabolic balance and inflammatory processes.²⁷ The PPAR α subtype is mainly expressed in tissues with high β -oxidation rates, such as the liver, brown adipose tissue, heart, and kidney, and is considered the master regulator of fatty acid catabolism, gluconeogenesis, and ketone body synthesis in a nutrition-dependent manner.^{27,28} Comparably, PPAR δ is involved in fatty acid uptake and oxidation, blood glucose homeostasis, and thermogenesis. It is ubiquitously expressed with main functions in skeletal muscles and brown adipose tissue.^{27,29,30} Both PPAR α and PPAR δ are closely linked to metabolic disorders, such as diabetes, cardiovascular disorders, nonalcoholic fatty liver disease (NAFLD), dyslipidemia, and obesity.^{30–32}

Here, we report the development of potent photoswitchable ligands for PPAR α and PPAR δ , extending the reach of photopharmacology to the remaining members of the important PPAR subfamily of nuclear receptors. Using a novel cellular test system embedding fluorescent reporter genes, we demonstrate a

Received: May 4, 2021

Published: July 2, 2021

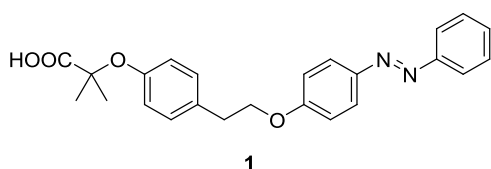


photoswitchable, time-resolved control of PPAR activation with these new photohormones in living cells.

RESULTS AND DISCUSSION

Owing to their superior photophysical properties, stability over multiple light-switching cycles, compatibility with various scaffolds, and ease of synthesis, azobenzenes have emerged as the most widely used compound class in photopharmacology.² Additionally, the photoswitching of azobenzenes employed in amphiphilic molecules is ideally suited to achieve reversible photoswitchable properties.³³ Based on these considerations, we employed GL479^{34,35} (**1**, Chart 1) as a lead compound, since it

Chart 1. Lead Compound pan-PPAR Agonist GL479 (**1**)

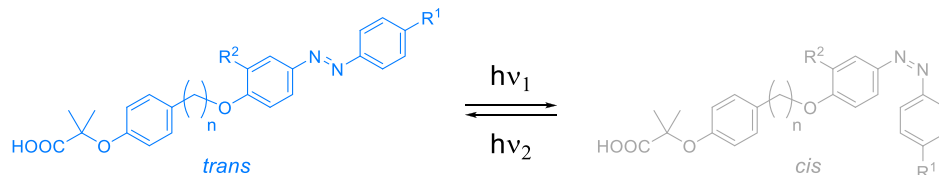


already contains an azobenzene linker but has not been previously investigated in a light-dependent fashion and was exclusively studied in the dark-adapted *trans*-form. GL479 (**1**) is a moderately potent pan-PPAR agonist with balanced potencies

on all PPARs but with a slight functional preference (higher efficacy) for the PPAR δ subtype (Table 1). Using light of wavelength $\lambda = 365$ nm for photoswitching, we also probed PPAR activation by the *cis*-isomer of **1**, which exhibited similar activity on all subtypes except a slight *trans*-preference for PPAR δ .

Co-crystal structures of the PPAR α (PDB ID: 4CI4) and PPAR γ (PDB ID: 4CI5)³⁶ ligand binding domains (LBDs) in complex with **1** were available for structure-based optimization. To obtain structural insights for PPAR δ , we employed molecular docking using a high-resolution PPAR δ co-crystal structure with a close analogue of the PPAR δ selective agonist GW501516³⁷ (PDB ID: 5Y7X)^{38,39} as a template. Initially, we studied the chain length of the alkoxy linker between the aromatic systems for potential optimization of the scaffold (Figure S1). Shortening by one carbon (**2**) appeared to be well-tolerated, while the further shortened diphenylether failed to span the ample binding pocket. As a result, the methyl propionate side chain was not properly placed in the lipophilic subpocket of PPAR α formed by Phe273, Val444, Leu456, and Leu460, but its methyl decoration clashed with His440. The extended chain of the phenoxypropyl analogue of **1**, in contrast, was too long causing a twisted conformation and a clash with Ser280. The phenoxyethyl (**1**) and phenoxyethyl (**2**) linkers were hence favored according to the docking studies.

Table 1. PPAR Modulatory Activity of GL479 (**1**) and Derivatives 2–11^a



#	R ¹	R ²	n	conf.	EC ₅₀ [μ M] (max. rel. act. [%])		
					PPAR α	PPAR γ	PPAR δ
1 (GL479)	-H	-H	2	<i>trans</i>	1.09 \pm 0.02 (31 \pm 1)	2.67 \pm 0.16 (25 \pm 1)	2.2 \pm 0.1 (61 \pm 2)
				<i>cis</i>	0.8 \pm 0.2 (29 \pm 2)	6.0 \pm 0.6 (28 \pm 2)	6 \pm 1 (34 \pm 6)
2	-H	-H	1	<i>trans</i>	3.7 \pm 0.3 (40 \pm 3)	5.40 \pm 0.07 (23 \pm 1)	2.8 \pm 0.3 (40 \pm 3)
				<i>cis</i>	3.5 \pm 0.7 (28 \pm 3)	6.6 \pm 0.3 (22 \pm 1)	4.1 \pm 0.2 (26 \pm 1)
3	-CH ₃	-H	2	<i>trans</i>	0.66 \pm 0.07 (24 \pm 1)	EC ₅₀ > 10 μ M (toxic \geq 6 μ M)	1.42 \pm 0.09 (33 \pm 1)
				<i>cis</i>	1.1 \pm 0.2 (22 \pm 3)	EC ₅₀ > 10 μ M	3.8 \pm 0.8 (31 \pm 5)
4	-Cl	-H	2	<i>trans</i>	0.79 \pm 0.09 (26 \pm 1)	3.2 \pm 1.3 (14 \pm 1)	8 \pm 2 (39 \pm 6)
				<i>cis</i>	1.1 \pm 0.2 (24 \pm 2)	EC ₅₀ > 10 μ M	8.1 \pm 0.4 (28 \pm 1)
5	-CH(CH ₃) ₂	-H	2	<i>trans</i>	0.47 \pm 0.01 (25 \pm 1)	2.1 \pm 0.2 (54 \pm 3)	1.77 \pm 0.07 (40 \pm 1)
				<i>cis</i>	0.28 \pm 0.05 (19 \pm 2)	2.6 \pm 0.2 (17 \pm 1)	3.4 \pm 0.2 (22 \pm 1)
6	-H	-CH ₃	2	<i>trans</i>	0.0070 \pm 0.0006 (38 \pm 1)	1.2 \pm 0.1 (20 \pm 1)	0.54 \pm 0.04 (45 \pm 1)
				<i>cis</i>	0.24 \pm 0.02 (43 \pm 1)	1.7 \pm 0.8 (24 \pm 1)	3.0 \pm 0.5 (41 \pm 4)
7	-H	-Cl	2	<i>trans</i>	0.029 \pm 0.004 (49 \pm 2)	0.82 \pm 0.07 (14 \pm 1)	0.24 \pm 0.02 (46 \pm 1)
				<i>cis</i>	0.040 \pm 0.003 (45 \pm 1)	0.92 \pm 0.08 (22 \pm 1)	0.35 \pm 0.06 (44 \pm 2)
8	-H	-CF ₃	2	<i>trans</i>	0.009 \pm 0.002 (46 \pm 2)	0.6 \pm 0.1 (34 \pm 2)	0.14 \pm 0.01 (45 \pm 2)
				<i>cis</i>	0.071 \pm 0.007 (42 \pm 1)	0.77 \pm 0.07 (32 \pm 1)	0.31 \pm 0.03 (37 \pm 2)
9	-CH ₃	-CH ₃	2	<i>trans</i>	0.036 \pm 0.006 (34 \pm 2)	2.3 \pm 0.1 (77 \pm 2)	0.12 \pm 0.01 (47 \pm 1)
				<i>cis</i>	0.64 \pm 0.08 (26 \pm 2)	1.2 \pm 0.3 (23 \pm 2)	0.8 \pm 0.1 (32 \pm 1)
10	-CH ₃	-CF ₃	2	<i>trans</i>	0.07 \pm 0.01 (87 \pm 5)	1.2 \pm 0.2 (65 \pm 5)	0.113 \pm 0.004 (43 \pm 1)
				<i>cis</i>	0.19 \pm 0.01 (41 \pm 1)	1.3 \pm 0.2 (33 \pm 2)	0.41 \pm 0.09 (40 \pm 6)
11	-CH ₃	-Cl	2	<i>trans</i>	0.04 \pm 0.01 (76 \pm 8)	4.5 \pm 0.2 (68 \pm 2)	0.12 \pm 0.02 (65 \pm 4)
				<i>cis</i>	0.29 \pm 0.05 (41 \pm 4)	4.8 \pm 0.4 (42 \pm 2)	0.38 \pm 0.03 (35 \pm 2)

^aActivities were determined in uniform Gal4 hybrid reporter gene assays in HEK293T cells. Maximum relative activation (max. rel. act.) refers to the activity of the respective reference agonist (PPAR α : GW7647; PPAR γ : pioglitazone; PPAR δ : L165,041; each at 1 μ M). Data are the mean \pm standard deviation (SD), $n \geq 3$.

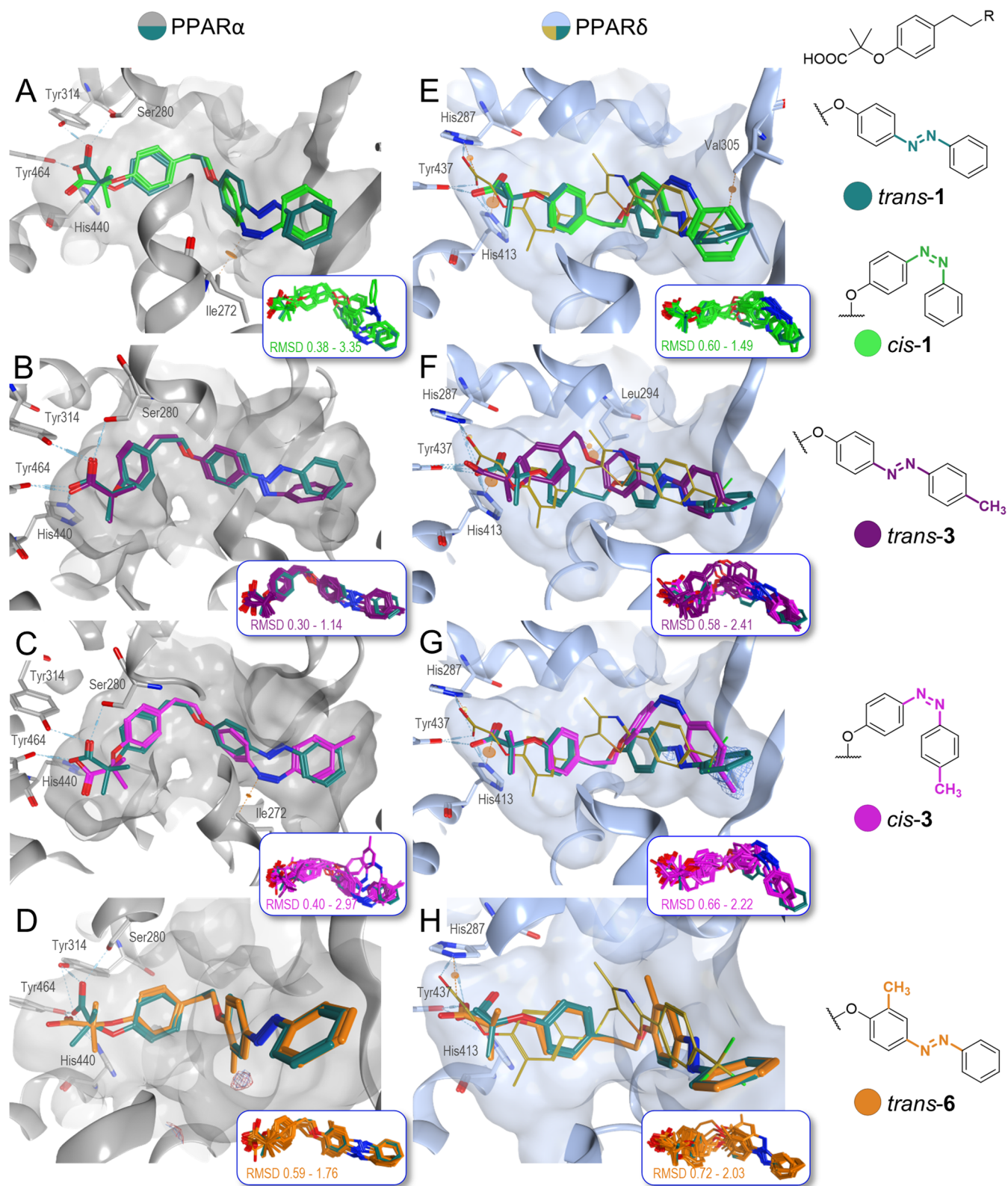
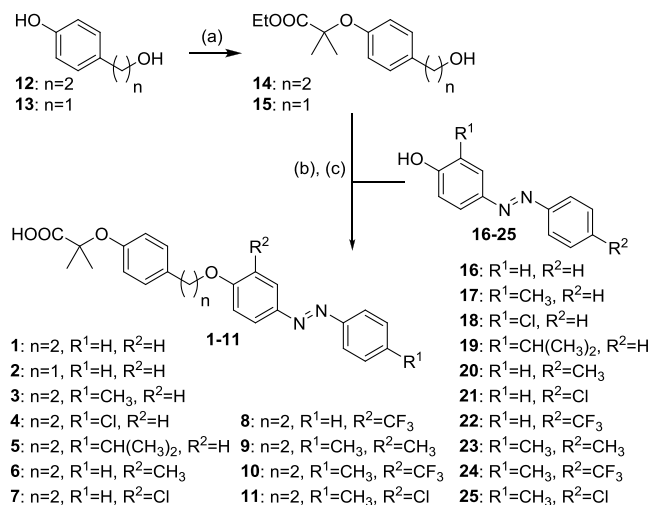


Figure 1. Molecular docking of 1, 3, and 6 to reveal optimization potential. *Trans*-1 (teal) is shown in all models for comparison. (A–D) PPAR α binding site (gray) from the co-crystal structure with lead 1 (teal, PDB ID: 4CI4³⁶) and (E–H) PPAR δ pocket (light blue) with the docked lead structure 1 for comparison (PDB ID: 5Y7X³⁸). The insets show overlays of the top 10 binding poses for each structure with their respective root-mean-square deviation (RMSD) range to the pose shown in the binding site. Docking of *cis*-1 (green, A and E) suggested that binding of the *cis*-counterpart is not favored. Terminal elongation with a *p*-methyl group enables improved binding modes of 3 in *trans*- (purple, B and F) and *cis*-states (magenta, G). An *o*-methyl residue introduced in 6 (orange, D and H) extends into a lipophilic cavity. Also see Figures S1 and S2.

In line with the activities observed *in vitro*, docking of **1** in *trans*- and *cis*-states revealed slightly unfavorable binding modes for the *cis*-counterpart with clashes of the azo linker (Figure 1A) and the terminal phenyl ring (Figure 1E). No clashes were observed for the shortened analogue *cis*-2, and several sound binding poses were predicted (Figure S1). These computational observations suggested **1** as a preferable lead for the development of *trans*-selective analogues and that *trans*-binding might be optimized by extension in the *para*-position of the terminal ring to hinder *cis*-binding (Figure 1C,G). Introduction of a methyl group in the *para*-position was well-tolerated by PPAR α as *trans*-3 and the co-crystallized ligand aligned well (Figure 1B). However, molecular docking of the extended *trans*-3 to the PPAR δ ligand binding site revealed its *cis*-counterpart *cis*-3 as the two top-ranked poses (Figures 1F,G and S2A). This observation together with high-energy barriers for *cis/trans*-isomerization of 43–52 kcal/mol in the forcefield used for the calculations (Amber10:EHT, Figure S3A,B) suggested less preference of PPAR δ for *trans*-binding. Further structural analysis indicated that introduction of methyl, chlorine, or trifluoromethyl modifications in the *ortho*-position of the central phenyl ring would address unoccupied space in the binding sites of PPAR α and PPAR δ to enhance affinity (Figure 1D,H). Especially in PPAR α , introduction of a methyl group in the *ortho*-position (**6**) seemed favorable as the moiety extended toward a lipophilic subpocket (Figures 1D and S2B).

Following these computational observations, we studied analogues **2–11** for improved optical control of PPAR α and PPAR δ (Scheme 1). All photohormone candidates **1–11** were

Scheme 1. Synthesis of **1–11**^a



^aReagents and conditions: (a) ethyl 2-bromo-2-methylpropanoate, K₂CO₃, DMF, reflux, 4 h, 47–80%; (b) azobenzenes **16–25**, PPh₃, DEAD, THF, room temperature (rt), 16 h; and (c) NaOH, EtOH, rt, 16 h, 20–93% over two steps.

obtained from the respective esters **14** and **15** following an S_N2 reaction of the phenols **12** and **13** with ethyl 2-bromo-2-methylpropanoate and K₂CO₃ in dimethylformamide (DMF) as previously reported.³⁴ The Mitsunobu reaction of **14** and **15** with the commercially available azobenzenes **16–25** using triphenylphosphine and diethyl azodicarboxylate (DEAD) in tetrahydrofuran (THF) and subsequent saponification of the obtained esters under basic conditions gave the desired carboxylic acids **1–11** (Scheme 1).

The biological evaluation of the photoswitchable ligands for PPAR modulation was performed in uniform hybrid Gal4 reporter gene assays in HEK293T cells. These test systems utilize chimeric constructs composed of the respective human nuclear receptor LBD and the DNA-binding domain of the Gal4 protein derived from yeast. Gal4-responsive firefly luciferase was used as a reporter gene, and constitutively expressed *Renilla* luciferase served for normalization and to monitor test compound toxicity. GW7647, Pioglitazone, and L165,041 (each at 1 μM) served as reference agonists for the three PPAR isoforms α, γ, and δ, respectively, to obtain the relative activation efficacy of the test compounds. To characterize both isomers of **1–11** individually, all assays were conducted with the *trans*-isomers in the dark and with the preilluminated *cis*-isomers (λ = 365 nm) using a Cell DISCO^{40,41} system during incubation. The biological activity of **1–11** is shown in Table 1.

Profiling of the lead compound GL479 (**1**) revealed agonism on all three PPAR isoforms with low micromolar EC₅₀ values in consistence with the previously reported data for PPAR α and γ.^{34,35} The *trans*-**1** and *cis*-**1** isomers exhibited comparable activity, except for a weak preference for *trans*-**1** on PPAR δ . Aiming to improve upon the potency, subtype-selectivity, and *trans*-preference of this new photohormone chemotype, we systematically varied the structural features of **1** suggested by molecular docking to hold optimization potential. Chain shortening by one carbon in *cis/trans*-**2** slightly reduced potency, thereby not evolving as a preferred modification and was not further pursued. Extension in the *para*-position of the terminal phenyl motif of **1** with methyl- (**3**) and chloro- (**4**) substituents hardly affected potency but slightly improved the desired *trans*-preference on PPAR α . The isopropyl analogue **5**, in contrast, was slightly more active on PPAR α than **1** with a preference for the *cis*-conformation. Additionally, the *para*-modifications (**3–5**) moderately improved selectivity over PPAR γ . Overall, **3–5** failed to provide a marked structural optimization. Hence, we focused our attention on the *ortho*-position of the central phenyl motif (**6–8**). As suggested by molecular docking, introduction of a methyl group (**6**) provided a remarkable improvement in PPAR α agonism, which was accompanied by a pronounced preference for *trans*-**6**. This modification was also favored by PPAR δ in terms of potency and *trans*-preference despite a smaller impact. Activity on PPAR γ was not affected, resulting in strongly improved selectivity over this PPAR subtype. A chlorine atom in the *ortho*-position (**7**) increased potency on PPAR α and PPAR δ as well, but *trans*-preference was lost. Trifluoromethyl analogue **8** was also very potent on PPAR α and exhibited a 10-fold preference for the *trans*-state but was not superior to **6**. On PPAR δ , trifluoromethyl substitution (**8**) evolved as the most favored modification in terms of potency. In an attempt to fuse the terminal (**3–5**) and central modifications (**6–8**) of the GL479 scaffold, we first combined methyl groups in both positions (**9**), resulting in a potent dual PPAR α/δ agonist with pronounced *trans*-preference but moderate activation efficiency. The combination of the terminal methyl motif with a trifluoromethyl group on the central ring (**10**) markedly improved activation efficiency with a slight loss in potency on PPAR α and less *trans*-preference while a chlorine atom on the central ring (**11**) resulted in balanced high potency on PPAR α/δ with strong activation efficiency and higher *trans*-preference. Additionally, **11** was selective for PPAR α/δ over PPAR γ . Overall, the computer-aided structural refinement of GL479 (**1**) as a photohormone yielded the highly potent and selective photoswitchable PPAR α agonist **6** (Figure

2A,B) and the dual PPAR α / δ photohormone **11**, which was equally equipped with favorable potency and selectivity (Figure

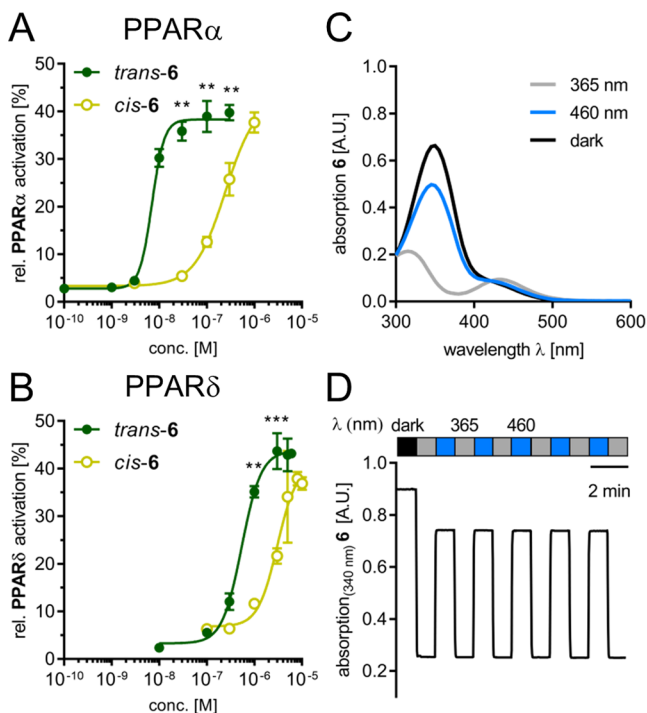


Figure 2. Characterization of photohormone **6**. Dose–response curves in cellular Gal4-PPAR α (A) or Gal4-PPAR δ (B) hybrid reporter gene assays in HEK293T cells. *Cis-6* was preilluminated ($\lambda = 365$ nm, 3 min) and maintained in *cis*-state with a Cell DISCO system.^{40,41} Relative activation refers to 1 μ M GW7647 (PPAR α) or L165,041 (PPAR δ). Data are the mean \pm SD, $n \geq 3$. ** $p < 0.01$ and *** $p < 0.001$ (t -test vs *cis-6*). Photophysical characteristics of **6**: UV–vis absorption scans (C, 50 μ M in dimethyl sulfoxide (DMSO)) in dark-adapted (*trans*, black), 460 nm adapted (*trans*, blue), and 365 nm adapted (*cis*, gray) photostationary states. (D) Reversible cycling (50 μ M in DMSO) with alternating illumination at 365 and 460 nm.

S4A,B). The PPAR α selective photohormone **6** additionally revealed high stability against microsomal degradation with an in vitro half-life of 103 ± 20 min (Figure S5), suggesting favorable metabolic stability and potential for in vivo applications.

Photophysical characterization of the new photohormones **6** and **11** by UV–vis spectroscopy upon illumination with $\lambda = 460$ nm (*trans*, blue) and $\lambda = 365$ nm (*cis*, gray) confirmed wavelength-dependent switching (Figures 2C and S4C), and repeated photoswitching over multiple cycles demonstrated high photostability (Figures 2D and S4D; 1 in Figure S3C,D).

Intrigued by the favorable activity profile and photophysical properties of the photohormones **6** and **11**, we studied their applicability as tools in a cellular setting. To reflect spatiotemporal control as a key feature of photopharmacology, we established a new cellular assay to observe time-resolved nuclear receptor activation and reversible activity of photohormones in intact living cells over a long time period.

For this, we used Gal4-responsive fluorescent mCherry or enhanced green fluorescent protein (eGFP) expression constructs as reporter genes in HEK293T cells. After transient transfection with the reporter and Gal4-PPAR α , cells were treated with photohormone **6** (Figure 3A). Light ($\lambda = 460$ and 365 nm) was used for switching between *cis*- and *trans*-conformations, and a Cell DISCO system^{40,41} (75 ms light

pulses every 15 s) served to maintain the *cis*-conformation while using a minimal nontoxic light dose. mCherry fluorescence was measured every hour starting 8 h after addition of **6** (10 nM). When cells were treated with *trans-6*, a constant increase in mCherry fluorescence was observed between 8 and 24 h after incubation (Figure 3A, blue curve). When cells were initially treated with *cis-6* for 8 h before switching to the *trans*-counterpart, the mCherry signal was markedly delayed (Figure 3A, red curve). By contrast, when cells were initially treated with *trans-6* before switching to the *cis*-form after 8 h, the mCherry signal initially increased similar to pure *trans-6* treatment for 2 h and then reached a low plateau with no further increase (Figure 3A, green curve). Similar observations were made with photohormone **11** on Gal4-PPAR δ (Figure S6A). Hence, photohormones **6** and **11** enable spatiotemporal control of the transcription factors PPAR α and PPAR δ .

Next, we studied selective and dual optical control of PPAR α and PPAR δ in a similar setting (Figure 3B). HEK293T cells were transiently transfected with Gal4-responsive mCherry and Gal4-PPAR α or Gal4-responsive eGFP and Gal4-PPAR δ . The cells were then pooled 5 h after transfection and treated with DMSO (0.1%), *cis*-/*trans-6*, or *cis*-/*trans-11*, and the fluorescence of mCherry and eGFP was determined after 40 h using a fluorescence microscope (Figures 3B, S6B, and S7). DMSO-treated cells revealed almost no mCherry or eGFP fluorescence. *Trans-6* at 10 nM markedly induced mCherry expression while *cis-6* had almost no effect, demonstrating optical control of PPAR α activity. At a higher concentration (300 nM), the mCherry signals were similar for *cis*- and *trans-6*, and slight eGFP fluorescence indicated weak PPAR δ activation. Hence, the photohormone **6** allows for strong, selective, and light-dependent PPAR α activation at a low 10 nM concentration, qualifying **6** as an attractive tool for photopharmacology.

CONCLUSIONS

Photohormones have evolved as a new attractive type of tool compounds that enable light-dependent modulation of transcription factors to achieve spatiotemporal control of transcriptional activity. As shown by our live-cell fluorescence reporter gene assay, this allows for photoswitching between transcriptionally active and inactive states, hence presenting photohormones as valuable in vitro tools for functional studies. In the field of nuclear receptors, temporal control appears particularly relevant since these (hormone) receptors are endogenously activated by short-lived molecules such as hormones and reactive metabolites. Hence, nuclear receptors are shortly stimulated under physiological conditions, which can be unmatched mimicked with photohormones. The importance of time in nuclear receptor modulation is further highlighted by their involvement in the circadian clock. Beyond this, optical control of nuclear receptor activity may also gain therapeutic relevance as it opens an avenue to local activation and inactivation, for example, with wirelessly powered and biodegradable optoelectronics to convert photohormones between active and inactive conformations in certain tissues.⁴² This may enable reduction of target-mediated adverse effects that cannot be avoided by conventional structural optimization to improve selectivity. Photohormones, in contrast, can be on-site activated or deactivated to spare tissues in which the target of interest mediates side effects. In vivo studies have shown that such optical control has therapeutic potential in metabolic diseases⁴³ and cancer.^{40,44}

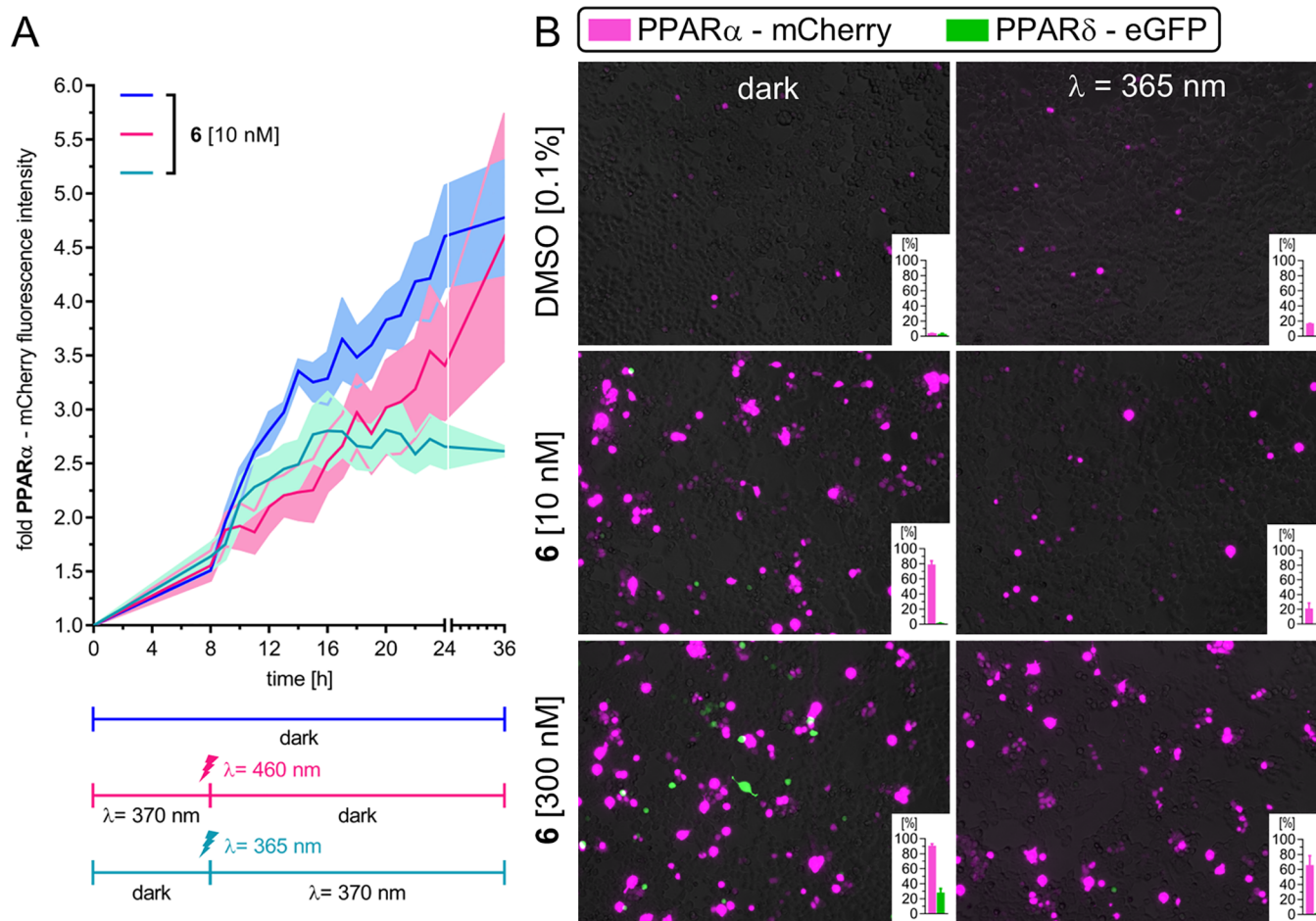


Figure 3. Spatiotemporal control of PPAR α by **6**. (A) Time-dependent PPAR α activation by **6** using an mCherry fluorescence reporter in live HEK293T cells. *Trans-6* was maintained in the dark (blue). Switching between the *cis*- and *trans*-isomers after 8 h was performed by illumination with $\lambda = 460$ nm (red) or $\lambda = 365$ nm (green) for 3 min, with subsequent maintenance of the *cis*-state using the Cell DISCO system.^{40,41} Fold fluorescence intensity refers to 0.1% DMSO. Lines, mean; shadows, standard error of the mean (SEM); $n = 3$. (B) Live-cell imaging of PPAR α -dependent mCherry reporter induction by *trans-6* (dark) and *cis-6* ($\lambda = 365$ nm). The PPAR δ -dependent eGFP fluorescence is negligible. The insets show mean \pm SEM relative reporter expression compared to GW7647 (PPAR α) or L165,041 (PPAR δ), $n = 2$.

Following these considerations, we have developed a highly potent and selective PPAR α photophormone from the weak pan-PPAR agonist GL479 (**1**) in a structure-guided fashion. The resulting analogue **6** not only exceeds the template compound **1** in terms of potency (factor > 150) and selectivity on PPAR α but is also equipped with the ability to be switched off by light-induced isomerization to its *cis*-conformer, which is less active on the intended target by a factor of 35. By enabling selective optical control of PPAR α , the photophormone **6** valuably expands the photopharmacology toolbox for nuclear receptors, enabling unprecedented in vitro and in cellulo experiments.

EXPERIMENTAL SECTION

Chemistry. General. All reagents and solvents were purchased from commercial sources (Sigma-Aldrich, TCI Europe N.V., Strem Chemicals, etc.) and used without further purification unless otherwise noted. Reactions were monitored by TLC on precoated, Merck silica gel 60 F_{254} glass-backed plates. Flash silica gel chromatography was performed using silica gel (SiO₂, particle size 40–63 μ m) purchased from Merck. All NMR spectra were measured on a Bruker Avance III HD 400 spectrometer (equipped with a CryoProbe). Multiplicities in the following experimental procedures are abbreviated as follows: s = singlet, d = doublet, t = triplet, q = quartet, quint = quintet, sext = sextet, hept = heptet, br = broad, and m = multiplet. Proton chemical shifts are expressed in parts per million (ppm, δ scale) and are referenced to the

residual protium in the NMR solvent (CDCl₃: $\delta = 7.26$; DMSO-*d*₆: $\delta = 2.50$; THF-*d*₈: $\delta = 1.72$). Carbon chemical shifts are expressed in ppm (δ scale) and are referenced to the carbon resonance of the NMR solvent (CDCl₃: $\delta = 77.16$; DMSO-*d*₆: $\delta = 39.52$; THF-*d*₈: $\delta = 25.31$). High-resolution mass spectra (HRMS) were obtained with an Agilent 6224 accurate mass time-of-flight (TOF) liquid chromatography/mass spectrometry (LC/MS) system using either an electrospray ionization (ESI) or atmospheric pressure chemical ionization (APCI) ion source. All reported data refer to the positive ionization mode. The compound purity was analyzed by high-performance liquid chromatography-ultraviolet (HPLC-UV) detection, and all compounds used for biological characterization had a purity $\geq 95\%$.

Synthesis and Analytical Characterization of **6 and **11** and Their Precursor **14**.** (*E*)-2-Methyl-2-(4-(2-(2-methyl-4-(phenyldiazenyl)phenoxy)ethyl)phenoxy)propanoic acid (**6**). Ethyl 2-(4-(2-hydroxyethyl)phenoxy)-2-methylpropanoate⁴⁵ (**14**, 20.0 mg, 79.3 mmol, 1.00 equiv), (*E*)-2-methyl-4-(phenyldiazenyl)phenol (**20**, 21.9 mg, 103 mmol, 1.30 equiv), and triphenylphosphine (27.0 mg, 103 mmol, 1.30 equiv) were dissolved in anhydrous THF (0.5 mL). DEAD (44.6 mg, 103 mmol, 1.30 equiv, 40% solution in toluene) was added dropwise at 0 °C. The mixture was stirred at rt overnight. The solvent was removed under reduced pressure. The crude was dissolved in EtOH, and 1M NaOH was added. The reaction was stirred at rt for 16 h. The solvent was removed under reduced pressure, and water was added and acidified with 1 M HCl. The mixture was extracted with CH₂Cl₂, dried over Na₂SO₄, filtered, and concentrated under reduced pressure.

The crude product was purified using flash column chromatography (CH_2Cl_2 to 20% MeOH in CH_2Cl_2) to yield **6** (28.2 mg, 67.4 μmol , 85%) as an orange solid. $^1\text{H NMR}$ (400 MHz, $\text{THF}-d_8$): δ = 7.84 (d, J = 7.3 Hz, 2H), 7.74 (s, 2H), 7.46 (t, J = 7.4 Hz, 2H), 7.40 (d, J = 7.1 Hz, 1H), 7.19 (d, J = 8.5 Hz, 2H), 7.05–6.99 (m, 1H), 6.84 (d, J = 8.5 Hz, 2H), 4.30–4.19 (m, 2H), 3.06 (t, J = 6.9 Hz, 2H), 2.25 (s, 3H), 1.52 (s, 6H). $^{13}\text{C NMR}$ (100 MHz, $\text{THF}-d_8$): δ = 175.6, 160.8, 155.7, 153.9, 147.4, 132.6, 131.0, 130.5, 129.8, 128.1, 124.8, 124.6, 123.3, 120.1, 111.5, 79.5, 70.1, 35.8, 25.9, 16.6. HRMS: m/z calcd for $\text{C}_{25}\text{H}_{27}\text{N}_2\text{O}_4^+$ ($[\text{M} + \text{H}]^+$): 419.1965; found, 419.1963.

(*E*)-2-(4-(2-(2-Chloro-4-(*p*-tolylidiazanyl)phenoxy)ethyl)phenoxy)-2-methylpropanoic acid (**11**). Ethyl 2-(4-(2-hydroxyethyl)phenoxy)-2-methylpropanoate (**14**, 21.9 mg, 87.0 μmol , 1.00 equiv), (*E*)-2-chloro-4-(*p*-tolylidiazanyl)phenol (**25**, 30.0 mg, 113 μmol , 1.30 equiv), and triphenylphosphine (29.6 mg, 113 μmol , 1.30 equiv) were dissolved in anhydrous THF (0.5 mL). DEAD (49.1 mg, 113 μmol , 1.30 equiv, 40% solution in toluene) was added dropwise at 0 °C. The mixture was stirred at rt overnight. The solvent was removed under reduced pressure. The crude was dissolved in EtOH, and 1 M NaOH was added. The reaction was stirred at rt for 16 h. The solvent was removed under reduced pressure, and water was added and acidified with 1 M HCl. The mixture was extracted with CH_2Cl_2 , dried over Na_2SO_4 , filtered, and concentrated under reduced pressure. The crude product was purified using flash column chromatography (CH_2Cl_2 to 20% MeOH in CH_2Cl_2) to yield **11** (17.6 mg, 38.9 μmol , 45%) as an orange solid. $^1\text{H NMR}$ (400 MHz, $\text{DMSO}-d_6$): δ = 7.94–7.85 (m, 2H), 7.78 (d, J = 8.3 Hz, 2H), 7.39 (dd, J = 8.6, 3.8 Hz, 3H), 7.27 (d, J = 8.7 Hz, 2H), 6.78 (d, J = 8.6 Hz, 2H), 4.34 (t, J = 6.9 Hz, 2H), 3.11–3.01 (m, 2H), 2.40 (s, 3H), 1.49 (s, 6H). $^{13}\text{C NMR}$ (101 MHz, $\text{DMSO}-d_6$): δ = 175.1, 156.0, 153.9, 149.9, 145.9, 141.6, 130.9, 130.0, 129.9, 124.9, 122.5, 122.5, 122.1, 118.4, 113.8, 78.3, 69.8, 33.9, 25.0, 21.0. HRMS: m/z calcd for $\text{C}_{25}\text{H}_{26}\text{ClN}_2\text{O}_4^+$ ($[\text{M} + \text{H}]^+$): 453.1576; found, 453.1573.

Ethyl 2-(4-(2-hydroxyethyl)phenoxy)-2-methylpropanoate (**14**). 4-(Hydroxyethyl)phenol (**12**, 200 mg, 1.45 mmol, 1.00 equiv) and K_2CO_3 (2.00 g, 14.5 mmol, 10.0 equiv) were dissolved in DMF (4.5 mL). Ethyl 2-bromo-2-methylpropanoate (875 mg, 4.48 mmol, 3.10 equiv) was added, and the mixture was stirred for 4 h under reflux. Water was added, phases were separated, and the aqueous layer was extracted with EtOAc, washed with brine, dried over Na_2SO_4 , filtered, and concentrated under reduced pressure. The crude product was purified using flash column chromatography (hexanes/EtOAc (8:2)) to yield **14** (292 mg, 1.16 mmol, 80%) as a colorless liquid. $^1\text{H NMR}$ (400 MHz, CDCl_3): δ = 7.13–7.05 (m, 2H), 6.83–6.76 (m, 2H), 4.24 (q, J = 7.1 Hz, 2H), 3.82 (t, J = 6.5 Hz, 2H), 2.80 (t, J = 6.6 Hz, 2H), 1.58 (s, 6H), 1.25 (d, J = 7.1 Hz, 3H). $^{13}\text{C NMR}$ (100 MHz, CDCl_3): δ = 174.5, 154.2, 132.1, 129.8, 119.6, 79.2, 63.9, 61.5, 38.5, 25.5, 14.2. HRMS: m/z calcd for $\text{C}_{14}\text{H}_{19}\text{O}_3^+$ ($[\text{M} - \text{H}_2\text{O}]^+$): 235.1329; found, 235.1335.

Photophysical Characterization. UV–vis spectra were recorded using a Varian Cary 50 Bio UV–visible spectrophotometer with BRAND Ultra-Micro UV-Cuvettes (10 mm light path). Switching was achieved using λ = 365 or 460 nm light-emitting diode (LED) light sources. The LEDs were pointed directly into the top of the sample cuvette. An initial spectrum of all photohormones (50 μM in DMSO) was recorded (dark-adapted state, black) and then again following illumination at λ = 365 nm for 1 min (*cis*-adapted state, gray). A third spectrum was recorded after irradiation at λ = 460 nm for 1 min (*trans*-adapted state, blue). To obtain the reversible *trans* \leftrightarrow *cis* spectrum, absorption at $\lambda_{\text{abs}} = 340$ nm was constantly measured, while alternating illumination at λ = 365 or 460 nm for the indicated times allowed for rapid isomerization of the photohormones (50 μM in DMSO). A mercury lamp with a power of 75 watts connected to a monochromator was directly pointed into the top of the sample cuvette, providing irradiation via an optic fiber cable with the two distinct wavelengths λ = 365 and 460 nm for 1 min each (absorption was read at $\lambda_{\text{abs}} = 340$ nm).

Computational Methods. *General.* Calculations were performed in Molecular Operating Environment (MOE, version 2020.09, Chemical Computing Group ULC, Montreal, QC, Canada) using

default settings for each tool/function unless stated otherwise. Amber10:EHT was used as the default forcefield for all calculations.

Molecular Docking. Docking was performed using the X-ray structures of the PPAR α LBD complexed with GL479 (PDB ID: 4CI4³⁶) and the PPAR δ LBD complexed with GW501516 derivative (PDB ID: 5Y7X³⁸). Protonation states of the complexes were adjusted using the MOE QuickPrep tool. The compounds were prepared using the Energy minimize tool and MOE Wash tool: protonation state dominant at pH 7.0. Docking was performed using the following settings in the MOE Dock tool: receptor: receptor + solvent; site: ligand atoms; placement: Triangle matcher; score: London dG; poses: 100; refinement: induced fit; refinement score: GBVI/WSA dG; poses: 10. As a pharmacophore query, the carboxylate oxygen of the respective crystallized ligand was set as an anionic H-bond acceptor feature with a 1.0 radius and one H-bond acceptor projection feature with a radius of 1.4 from the same atom. All 10 superimposed binding poses are shown as insets. The RMSD values between docked poses were calculated with the mol_rmsd SVL script in MOE and are displayed as min–max ranges. Redocking of the crystallized ligand GL479 (**1**) in PPAR α (PDB ID: 4CI4³⁶) resulted in an RMSD value of 0.1565 (range 0.1565–1.1580, mean 0.6668).

Torsion Profile. The minimized energies (in kcal/mol) of the associated lowest-energy structure were calculated for the conversion from *trans*- to *cis*-state of **1** and vice versa using the MOE torsion profile tool in bidirectional mode with both nitrogen atoms selected from the azo ($\text{N}=\text{N}$) double bond.

In Vitro Pharmacological Characterization. *Hybrid Reporter Gene Assays. Plasmids.* The Gal4-fusion receptor plasmids pFA-CMV-hPPAR α -LBD, pFA-CMV-hPPAR γ -LBD, and pFA-CMV-hPPAR δ -LBD coding for the hinge region and the ligand binding domain of the canonical isoform of the respective nuclear receptor have been reported previously.⁴⁶ pFR-Luc (Stratagene, La Jolla, CA) was used as the reporter plasmid and pRL-SV40 (Promega, Madison, WI) for normalization of transfection efficiency and cell growth.

Procedure. HEK293T cells were cultured in Dulbecco's modified Eagle's medium (DMEM), high glucose with 10% fetal calf serum (FCS), sodium pyruvate (1 mM), penicillin (100 U/mL), and streptomycin (100 $\mu\text{g}/\text{mL}$) at 37 °C and 5% CO_2 . Twenty-four hours before transfection, the cells were seeded in transparent 96-well plates (3×10^4 cells/well). Before transfection, the medium was changed to Opti-MEM without supplements. Transient transfection was carried out using Lipofectamine LTX reagent (Invitrogen, Carlsbad, CA) according to the manufacturer's protocol with pFR-Luc (Stratagene), pRL-SV40 (Promega), and the corresponding Gal4-fusion nuclear receptor plasmid. Five hours after transfection, the medium was changed to Opti-MEM supplemented with penicillin (100 U/mL) and streptomycin (100 $\mu\text{g}/\text{mL}$) and additionally containing 0.1% dimethyl sulfoxide (DMSO) and the respective test compound or 0.1% DMSO alone as the untreated control. Each concentration was tested in duplicate, and each experiment was repeated independently at least three times. After incubation overnight (14–16 h), the cells were assayed for luciferase activity using the Dual-Glo Luciferase Assay System (Promega) according to the manufacturer's protocol. Luminescence was measured with a Tecan Spark 10M luminometer (Tecan Deutschland GmbH, Crailsheim, Germany). Normalization of transfection efficiency and cell growth was done by dividing the firefly luciferase data by *Renilla* luciferase data and multiplying the value by 1000, resulting in relative light units (RLUs). Fold activation was obtained by dividing the mean RLU of the test compound by the mean RLU of the untreated control. Max. relative activation refers to the max fold activation by a test compound divided by the fold activation of the respective reference agonist (at a concentration of 1 μM). All hybrid assays were validated with the respective reference agonists (PPAR α : GW7647; PPAR γ : pioglitazone; PPAR δ : L165,041), which yielded EC₅₀ values in agreement with the literature. Characterization of the respective *cis*-counterparts was performed in the same way with preirradiated compounds (irradiation for 3 min at λ = 365 nm before incubation). To maintain the compound in the *cis*-adapted state, the Cell DISCO system was used during incubation with 75 ms light pulses (λ = 370 nm) every 15 s. For dose–response curve fitting and

calculation of EC_{50} values, the equation “[Agonist] vs response–variable slope (four parameters)” was performed with mean relative activations \pm SD using GraphPad Prism (version 7.00, GraphPad Software, La Jolla, CA).

Microsomal Stability Assay. The solubilized test compound **6** or 7-ethoxycoumarin as a reference (5 μ L, final concentration 10 μ M) was preincubated at 37 °C in 432 μ L of phosphate buffer (0.1 M, pH 7.4) together with 50 μ L of an NADPH regenerating system (30 mM glucose-6-phosphate, 4 U/mL glucose-6-phosphate dehydrogenase, 10 mM NADP, 30 mM $MgCl_2$). After 5 min, the reaction was started by the addition of 13 μ L of the microsome mix from the liver of Sprague–Dawley rats (Invitrogen; 20 mg protein/mL in 0.1 M phosphate buffer) in a shaking water bath at 37 °C. The reaction was stopped by adding 500 μ L of ice-cold methanol at 0, 15, 30, and 60 min. The samples were centrifuged at 5000g for 5 min at 4 °C, and the test compound was quantified from the supernatants using HPLC-UV detection. The composition of the mobile phase was adapted to the test compound in a range of MeOH 40–90% and water (0.1% formic acid) 10–60%; flow-rate: 1 mL/min; stationary phase: Purospher STAR, RP18, 5 μ m, 125 \times 4; precolumn: Purospher STAR, RP18, 5 μ m, 4 \times 4; detection wavelength: 254 and 280 nm; and injection volume: 50 μ L. Control samples were performed to check the test compound’s stability in the reaction mixture: the first control was without NADPH, which is needed for the enzymatic activity of the microsomes, the second control was with inactivated microsomes (incubated for 20 min at 90 °C), and the third control was without the test compound (to determine the baseline). The amounts of the test compound were quantified by an external calibration curve. Data are expressed as the mean \pm SEM of the remaining compound from three independent experiments. In vitro half-life was calculated by a logarithmic linear transformation of the remaining amounts of nonmetabolized test compound versus time in GraphPad Prism 7 as described previously.^{47,48}

Fluorescence Reporter Gene Assay. *Plasmids.* The Gal4-responsive fluorescence reporter mCherry was expressed from plasmid pUAS-mCherry-NLS (Addgene, entry 87695, Watertown, MA, U.S.A.).⁴⁹ The Gal4-fusion receptor plasmid pFA-CMV-hPPAR α -LBD and pFA-CMV-hPPAR δ -LBD coding for the hinge region and the ligand binding domain of the canonical isoform of the respective nuclear receptor have been reported previously.⁴⁶

Procedure. HEK293T cells were cultured in DMEM, high glucose with 10% FCS, sodium pyruvate (1 mM), penicillin (100 U/mL), and streptomycin (100 μ g/mL) at 37 °C and 5% CO_2 . Twenty-four hours before transfection, the cells were seeded in black cell culture 96-well microplates with μ Clear flat bottom (3 \times 10⁴ cells/well; Greiner Bio-One GmbH, Frickenhausen, Germany). Before transfection, the medium was changed to Opti-MEM without supplements. Transient transfection was carried out using Lipofectamine LTX reagent (Invitrogen) according to the manufacturer’s protocol with pUAS-mCherry-NLS (Addgene, entry 87695) and the corresponding Gal4-fusion nuclear receptor plasmid. Five hours after transfection, the medium was changed to Opti-MEM supplemented with penicillin (100 U/mL) and streptomycin (100 μ g/mL) and additionally containing 0.1% DMSO and the respective test compound or 0.1% DMSO alone as the untreated control. Each concentration was tested in duplicate, and each experiment was repeated independently three times. After incubation for 8 h, the living cells were assayed for fluorescence reporter intensity every hour until 24 h and at 36 h. The fluorescence intensity (FI) was measured after excitation at 585/10 nm with the emission wavelength of 610/10 nm in bottom reading mode with a Tecan Spark luminometer (Tecan Deutschland GmbH). Fold FI was obtained by dividing the mean FI of the test compound by the mean FI of the untreated control. Hybrid fluorescence assay performance was monitored with the respective reference agonists at a concentration of 1 μ M (PPAR α : GW7647; PPAR δ : L165,041). Characterization of the respective *cis*-counterparts was performed in the same way with preirradiated compounds (irradiation for 3 min at λ = 365 nm before incubation). To maintain the compound in the *cis*-adapted state, the Cell DISCO system was used during incubation with 75 ms light pulses (λ = 370 nm) every 15 s. For two of the three study arms,

photoswitching of the test compounds was conducted after 8 h of incubation with irradiation for 3 min at λ = 365 or 460 nm, respectively.

Fluorescence Cell Imaging. *Plasmids.* The Gal4-responsive fluorescence reporters mCherry and eGFP were expressed from the plasmids pUAS-mCherry-NLS (Addgene, entry 87695)⁴⁹ and pGRE-GFP (Addgene, entry 12516),⁵⁰ respectively. The Gal4-fusion receptor plasmid pFA-CMV-hPPAR α -LBD and pFA-CMV-hPPAR δ -LBD coding for the hinge region and the ligand binding domain of the canonical isoform of the respective nuclear receptor have been reported previously.⁴⁶

Procedure. HEK293T cells were cultured in DMEM, high glucose with 10% FCS, sodium pyruvate (1 mM), penicillin (100 U/mL), and streptomycin (100 μ g/mL) at 37 °C and 5% CO_2 . Twenty-four hours before transfection, cells were seeded in 24-well plates (1.5 \times 10⁵ cells/well). Before transfection, the medium was changed to Opti-MEM without supplements. Transient transfection was carried out using Lipofectamine LTX reagent (Invitrogen) according to the manufacturer’s protocol with the combination of pUAS-mCherry-NLS (Addgene, entry 87695) and pFA-CMV-hPPAR α -LBD or pGRE-GFP (Addgene, entry 12516) and pFA-CMV-hPPAR δ -LBD. Five hours after transfection, the cells transfected with pUAS-mCherry-NLS and pFA-CMV-hPPAR α -LBD or pGRE-GFP and pFA-CMV-hPPAR δ -LBD were trypsinized and pooled in a 50 mL tube, centrifuged, and resuspended in Opti-MEM supplemented with penicillin (100 U/mL) and streptomycin (100 μ g/mL). The transfected cells were then reseeded in 96-well plates already containing Opti-MEM with supplements and 0.1% DMSO and the respective test compound or 0.1% DMSO alone as the untreated control. Each concentration was performed in duplicate, and each experiment was repeated independently two times. Characterization of the respective *cis*-counterparts was performed in the same way with preirradiated compounds (irradiation for 3 min at λ = 365 nm before incubation). To maintain the compound in the *cis*-adapted state, the Cell DISCO system was used during incubation with 75 ms light pulses (λ = 370 nm) every 15 s.

Imaging. For the analysis of fluorescence reporter gene expression, images were acquired 40 h after incubation with the test compounds using a Zeiss Axio Observer Z1 (Carl Zeiss AG, Oberkochen, Germany) microscope equipped with a 10 \times objective lens. The filter sets had the following wavelengths/bandwidths: mCherry, excitation 545/40 nm ET bandpass; beam splitter T570 LPXR; and emission 620/60 nm ET bandpass; and eGFP, excitation 470/40 nm ET bandpass; beam splitter T495 LPXR; and emission 525/50 nm ET bandpass. Image analysis was performed with ImageJ software (version 1.53e). Integrated densities were measured from representative images in separated stacks (mCherry and eGFP channel) as RGB color images for the whole area, and relative integrated densities refer to mean integrated densities divided by the mean integrated density of the respective reference agonist (at a concentration of 1 μ M; PPAR α : GW7647; PPAR δ : L165,041).

■ ASSOCIATED CONTENT

Supporting Information

The Supporting Information is available free of charge at <https://pubs.acs.org/doi/10.1021/acs.jmedchem.1c00810>.

Supporting Information containing Figures S1–S7, Table S1, synthesis and analytical characterization of **1–11** and their precursors, HPLC traces, and NMR spectra (PDF)

Molecular formula strings containing molecular structures of **1–11** in *trans* and *cis* conformations and associated activity data (csv)

■ AUTHOR INFORMATION

Corresponding Authors

Dirk Trauner – Department of Chemistry, New York University, New York, New York 10003, United States;

orcid.org/0000-0002-6782-6056; Email: dirktrauner@nyu.edu

Nyul Merk – Institute of Pharmaceutical Chemistry, Goethe University Frankfurt, 60438 Frankfurt, Germany;

orcid.org/0000-0002-5359-8128; Email: merk@pharmchem.uni-frankfurt.de

Authors

Sabine Willems – Institute of Pharmaceutical Chemistry, Goethe University Frankfurt, 60438 Frankfurt, Germany

Johannes Morstein – Department of Chemistry, New York University, New York, New York 10003, United States

Konstantin Hinnah – Department of Chemistry, New York University, New York, New York 10003, United States

Complete contact information is available at:

<https://pubs.acs.org/10.1021/acs.jmedchem.1c00810>

Author Contributions

[§]S.W. and J.M. contributed equally to this study.

Notes

The authors declare no competing financial interest.

ACKNOWLEDGMENTS

pUAS-mCherry-NLS was a gift from Robert Campbell (Addgene plasmid no. 87695; <http://n2t.net/addgene:87695>; RRID:Addgene_87695). pGRE-GFP was a gift from Bert Vogelstein (Addgene plasmid no. 12516; <http://n2t.net/addgene:12516>; RRID:Addgene_12516). J.M. and K.H. thank the German Academic Scholarship Foundation for a fellowship. J.M. thanks the New York University for a Margaret and Herman Sokol fellowship and the NCI for an F99/K00 award (1F99CA253758-01). D.M. thanks the Aventis Foundation for financial support.

ABBREVIATIONS USED

DEAD, diethyl azodicarboxylate; eGFP, enhanced green fluorescent protein; ER, estrogen receptor; FI, fluorescence intensity; FXR, farnesoid X receptor; LBD, ligand binding domain; NAFLD, nonalcoholic fatty liver disease; NR, nuclear receptor; PPAR, peroxisome proliferator-activated receptor; RAR, retinoic acid receptor; RLU, relative light units; rt, room temperature

REFERENCES

- (1) Szymański, W.; Beierle, J. M.; Kistemaker, H. A. V.; Velema, W. A.; Feringa, B. L. Reversible Photocontrol of Biological Systems by the Incorporation of Molecular Photoswitches. *Chem. Rev.* **2013**, *113*, 6114–6178.
- (2) Broichhagen, J.; Frank, J. A.; Trauner, D. A Roadmap to Success in Photopharmacology. *Acc. Chem. Res.* **2015**, *48*, 1947–1960.
- (3) Hüll, K.; Morstein, J.; Trauner, D. In Vivo Photopharmacology. *Chem. Rev.* **2018**, *118*, 10710–10747.
- (4) Fuchter, M. J. On the Promise of Photopharmacology Using Photoswitches: A Medicinal Chemist's Perspective. *J. Med. Chem.* **2020**, *63*, 11436–11447.
- (5) Banghart, M.; Borges, K.; Isacoff, E.; Trauner, D.; Kramer, R. H. Light-Activated Ion Channels for Remote Control of Neuronal Firing. *Nat. Neurosci.* **2004**, *7*, 1381–1386.
- (6) Broichhagen, J.; Schönberger, M.; Cork, S. C.; Frank, J. A.; Marchetti, P.; Bugliani, M.; Shapiro, A. M. J.; Trapp, S.; Rutter, G. A.; Hodson, D. J.; Trauner, D. Optical Control of Insulin Release Using a Photoswitchable Sulfonyleurea. *Nat. Commun.* **2014**, *5*, No. 5116.
- (7) Broichhagen, J.; Damijonaitis, A.; Levitz, J.; Sokol, K. R.; Leippe, P.; Konrad, D.; Isacoff, E. Y.; Trauner, D. Orthogonal Optical Control

of a G Protein-Coupled Receptor with a SNAP-Tethered Photochromic Ligand. *ACS Cent. Sci.* **2015**, *1*, 383–393.

- (8) Morstein, J.; Dacheux, M. A.; Norman, D. D.; Shemet, A.; Donthamsetti, P. C.; Citir, M.; Frank, J. A.; Schultz, C.; Isacoff, E. Y.; Parrill, A. L.; Tigyi, G. J.; Trauner, D. Optical Control of Lysophosphatidic Acid Signaling. *J. Am. Chem. Soc.* **2020**, *142*, 10612–10616.
- (9) Prischich, D.; Gomila, A. M. J.; Milla-Navarro, S.; Sangüesa, G.; Diez-Alarcia, R.; Preda, B.; Matera, C.; Batlle, M.; Ramírez, L.; Giralt, E.; Hernando, J.; Guasch, E.; Meana, J. J.; de la Villa, P.; Gorostiza, P. Adrenergic Modulation With Photochromic Ligands. *Angew. Chem., Int. Ed.* **2021**, *60*, 3625–3631.
- (10) Quandt, G.; Höfner, G.; Pabel, J.; Dine, J.; Eder, M.; Wanner, K. T. First Photoswitchable Neurotransmitter Transporter Inhibitor: Light-Induced Control of γ -Aminobutyric Acid Transporter 1 (GAT1) Activity in Mouse Brain. *J. Med. Chem.* **2014**, *57*, 6809–6821.
- (11) Cheng, B.; Morstein, J.; Ladefoged, L. K.; Maesen, J. B.; Schiøtt, B.; Sinning, S.; Trauner, D. A Photoswitchable Inhibitor of the Human Serotonin Transporter. *ACS Chem. Neurosci.* **2020**, *11*, 1231–1237.
- (12) Cheng, B.; Shchepakina, D.; Kavanaugh, M. P.; Trauner, D. Photoswitchable Inhibitor of a Glutamate Transporter. *ACS Chem. Neurosci.* **2017**, *8*, 1668–1672.
- (13) Bonardi, F.; London, G.; Nouwen, N.; Feringa, B. L.; Driessen, A. J. M. Light-Induced Control of Protein Translocation by the SecYEG Complex. *Angew. Chem., Int. Ed.* **2010**, *49*, 7234–7238.
- (14) Velema, W. A.; Van Der Berg, J. P.; Hansen, M. J.; Szymanski, W.; Driessen, A. J. M.; Feringa, B. L. Optical Control of Antibacterial Activity. *Nat. Chem.* **2013**, *5*, 924–928.
- (15) Tsai, Y.-H.; Essig, S.; James, J. R.; Lang, K.; Chin, J. W. Selective, Rapid and Optically Switchable Regulation of Protein Function in Live Mammalian Cells. *Nat. Chem.* **2015**, *7*, 554–561.
- (16) Kol, M.; Williams, B.; Toombs-Ruane, H.; Franquelim, H. G.; Korneev, S.; Schroerer, C.; Schwill, P.; Trauner, D.; Holthuis, J. C.; Frank, J. A. Optical Manipulation of Sphingolipid Biosynthesis Using Photoswitchable Ceramides. *eLife* **2019**, *8*, No. e43230.
- (17) Gronemeyer, H.; Gustafsson, J. Å.; Laudet, V. Principles for Modulation of the Nuclear Receptor Superfamily. *Nat. Rev. Drug Discovery* **2004**, *3*, 950–964.
- (18) Aranda, A.; Pascual, A. Nuclear Hormone Receptors and Gene Expression. *Physiol. Rev.* **2001**, *81*, 1269–1304.
- (19) Morstein, J.; Impastato, A. C.; Trauner, D. Photoswitchable Lipids. *ChemBioChem* **2021**, *22*, 73–83.
- (20) Proschak, E.; Heitel, P.; Kalinowsky, L.; Merk, D. Opportunities and Challenges for Fatty Acid Mimetics in Drug Discovery. *J. Med. Chem.* **2017**, *60*, 5235–5266.
- (21) Morstein, J.; Awale, M.; Reymond, J. L.; Trauner, D. Mapping the Azolog Space Enables the Optical Control of New Biological Targets. *ACS Cent. Sci.* **2019**, *5*, 607–618.
- (22) Morstein, J.; Trads, J. B.; Hinnah, K.; Willems, S.; Barber, D. M.; Trauner, M.; Merk, D.; Trauner, D. Optical Control of the Nuclear Bile Acid Receptor FXR with a Photohormone. *Chem. Sci.* **2020**, *11*, 429–434.
- (23) Hinnah, K.; Willems, S.; Morstein, J.; Heering, J.; Hartrampf, F. W. W.; Broichhagen, J.; Leippe, P.; Merk, D.; Trauner, D. Photohormones Enable Optical Control of the Peroxisome Proliferator-Activated Receptor γ (PPAR γ). *J. Med. Chem.* **2020**, *63*, 10908–10920.
- (24) Tsuchiya, K.; Umeno, T.; Tsuji, G.; Yokoo, H.; Tanaka, M.; Fukuhara, K.; Demizu, Y.; Misawa, T. Development of Photoswitchable Estrogen Receptor Ligands. *Chem. Pharm. Bull.* **2020**, *68*, 398–402.
- (25) Evans, R. M.; Mangelsdorf, D. J. Nuclear Receptors, RXR, and the Big Bang. *Cell* **2014**, *157*, 255–266.
- (26) Unsworth, A. J.; Flora, G. D.; Gibbins, J. M. Non-Genomic Effects of Nuclear Receptors: Insights from the Anucleate Platelet. *Cardiovasc. Res.* **2018**, *114*, 645–655.
- (27) Michalik, L.; Auwerx, J.; Berger, J. P.; Chatterjee, V. K.; Glass, C. K.; Gonzalez, F. J.; Grimaldi, P. A.; Kadowaki, T.; Lazar, M. A.; O'Rahilly, S.; Palmer, C. N. A.; Plutzky, J.; Reddy, J. K.; Spiegelman, B. M.; Staels, B.; Wahli, W. International Union of Pharmacology. LXI.

Peroxisome Proliferator-Activated Receptors. *Pharmacol. Rev.* **2006**, *58*, 726–741.

(28) Pawlak, M.; Lefebvre, P.; Staels, B. Molecular Mechanism of PPAR α Action and Its Impact on Lipid Metabolism, Inflammation and Fibrosis in Non-Alcoholic Fatty Liver Disease. *J. Hepatol.* **2015**, *62*, 720–733.

(29) Tanaka, T.; Yamamoto, J.; Iwasaki, S.; Asaba, H.; Hamura, H.; Ikeda, Y.; Watanabe, M.; Magoori, K.; Ioka, R. X.; Tachibana, K.; Watanabe, Y.; Uchiyama, Y.; Sumi, K.; Iguchi, H.; Ito, S.; Doi, T.; Hamakubo, T.; Naito, M.; Auwerx, J.; Yanagisawa, M.; Kodama, T.; Sakai, J. Activation of Peroxisome Proliferator-Activated Receptor δ Induces Fatty Acid β -Oxidation in Skeletal Muscle and Attenuates Metabolic Syndrome. *Proc. Natl. Acad. Sci. U.S.A.* **2003**, *100*, 15924–15929.

(30) Liu, Y.; Colby, J.; Zuo, X.; Jaoude, J.; Wei, D.; Shureiqi, I. The Role of PPAR- δ in Metabolism, Inflammation, and Cancer: Many Characters of a Critical Transcription Factor. *Int. J. Mol. Sci.* **2018**, *19*, No. 3339.

(31) Ratziu, V.; Harrison, S. A.; Francque, S.; Bedossa, P.; Lehert, P.; Serfaty, L.; Romero-Gomez, M.; Boursier, J.; Abdelmalek, M.; Caldwell, S.; Drenth, J.; Anstee, Q. M.; Hum, D.; Hanf, R.; Roudot, A.; Megnier, S.; Staels, B.; Sanyal, A.; et al. Elafibranor, an Agonist of the Peroxisome Proliferator-Activated Receptor- α and - δ , Induces Resolution of Nonalcoholic Steatohepatitis Without Fibrosis Worsening. *Gastroenterology* **2016**, *150*, 1147–1159.e5.

(32) Bougarne, N.; Weyers, B.; Desmet, S. J.; Deckers, J.; Ray, D. W.; Staels, B.; De Bosscher, K. Molecular Actions of PPAR α in Lipid Metabolism and Inflammation. *Endocr. Rev.* **2018**, *39*, 760–802.

(33) Beharry, A. A.; Woolley, G. A. Azobenzene Photoswitches for Biomolecules. *Chem. Soc. Rev.* **2011**, *40*, 4422–4437.

(34) Giampietro, L.; D'Angelo, A.; Giancristofaro, A.; Ammazalorso, A.; De Filippis, B.; Fantacuzzi, M.; Linciano, P.; MacCallini, C.; Amoroso, R. Synthesis and Structure-Activity Relationships of Fibrate-Based Analogues inside PPARs. *Bioorg. Med. Chem. Lett.* **2012**, *22*, 7662–7666.

(35) Giampietro, L.; Laghezza, A.; Cerchia, C.; Florio, R.; Recinella, L.; Capone, F.; Ammazalorso, A.; Bruno, I.; De Filippis, B.; Fantacuzzi, M.; Ferrante, C.; MacCallini, C.; Tortorella, P.; Verginelli, F.; Brunetti, L.; Cama, A.; Amoroso, R.; Loidice, F.; Lavecchia, A. Novel Phenylidiazanyl Fibrate Analogues as PPAR $\alpha/\gamma/\delta$ Pan-Agonists for the Amelioration of Metabolic Syndrome. *ACS Med. Chem. Lett.* **2019**, *10*, 545–551.

(36) dos Santos, J. C.; Bernardes, A.; Giampietro, L.; Ammazalorso, A.; De Filippis, B.; Amoroso, R.; Polikarpov, I. Different Binding and Recognition Modes of GL479, a Dual Agonist of Peroxisome Proliferator-Activated Receptor α/γ . *J. Struct. Biol.* **2015**, *191*, 332–340.

(37) Oliver, W. R.; Shenk, J. L.; Snaith, M. R.; Russell, C. S.; Plunket, K. D.; Bodkin, N. L.; Lewis, M. C.; Winegar, D. A.; Sznajdman, M. L.; Lambert, M. H.; Xu, H. E.; Sternbach, D. D.; Kliewer, S. A.; Hansen, B. C.; Willson, T. M. A Selective Peroxisome Proliferator-Activated Receptor δ Agonist Promotes Reverse Cholesterol Transport. *Proc. Natl. Acad. Sci. U.S.A.* **2001**, *98*, 5306–5311.

(38) Kim, H. L.; Chin, J. W.; Cho, S. J.; Song, J. Y.; Yoon, H. S.; Bae, J. H. Design, synthesis, and the X-ray co-crystal structure of Highly Potent, Selective, and Orally Bioavailable, Novel Peroxisome Proliferator-Activated Receptor delta Agonists. 2018, PDB ID 5Y7X, DOI: [10.2210/pdb5Y7X/pdb](https://doi.org/10.2210/pdb5Y7X/pdb).

(39) Wu, C. C.; Baiga, T. J.; Downes, M.; La Clair, J. J.; Atkins, A. R.; Richard, S. B.; Fan, W.; Stockley-Noel, T. A.; Bowman, M. E.; Noel, J. P.; Evans, R. M. Structural Basis for Specific Ligation of the Peroxisome Proliferator-Activated Receptor δ . *Proc. Natl. Acad. Sci. U.S.A.* **2017**, *114*, E2563–E2570.

(40) Borowiak, M.; Nahaboo, W.; Reynders, M.; Nekolla, K.; Jalinot, P.; Hasserodt, J.; Rehberg, M.; Delattre, M.; Zahler, S.; Vollmar, A.; Trauner, D.; Thorn-Seshold, O. Photoswitchable Inhibitors of Microtubule Dynamics Optically Control Mitosis and Cell Death. *Cell* **2015**, *162*, 403–411.

(41) Morstein, J.; Trauner, D. Photopharmacological Control of Lipid Function. In *Methods in Enzymology*; Academic Press Inc., 2020; Vol. 638, pp 219–232.

(42) Morstein, J.; Trauner, D. New Players in Phototherapy: Photopharmacology and Bio-Integrated Optoelectronics. *Curr. Opin. Chem. Biol.* **2019**, *50*, 145–151.

(43) Mehta, Z. B.; Johnston, N. R.; Nguyen-Tu, M.-S.; Broichhagen, J.; Schultz, P.; Larner, D. P.; Leclerc, I.; Trauner, D.; Rutter, G. A.; Hodson, D. J. Remote Control of Glucose Homeostasis in Vivo Using Photopharmacology. *Sci. Rep.* **2017**, *7*, No. 291.

(44) Babii, O.; Afonin, S.; Garmanchuk, L. V.; Nikulina, V. V.; Nikolaienko, T. V.; Storozhuk, O. V.; Shelest, D. V.; Dasyukevich, O. I.; Ostapchenko, L. I.; Iurchenko, V.; Zozulya, S.; Ulrich, A. S.; Komarov, I. V. Direct Photocontrol of Peptidomimetics: An Alternative to Oxygen-Dependent Photodynamic Cancer Therapy. *Angew. Chem., Int. Ed.* **2016**, *55*, 5493–5496.

(45) Giampietro, L.; D'Angelo, A.; Giancristofaro, A.; Ammazalorso, A.; De Filippis, B.; Fantacuzzi, M.; Linciano, P.; Maccallini, C.; Amoroso, R. Synthesis and Structure-Activity Relationships of Fibrate-Based Analogues inside PPARs. *Bioorg. Med. Chem. Lett.* **2012**, *22*, 7662–7666.

(46) Rau, O.; Wurglics, M.; Paulke, A.; Zitzkowski, J.; Meindl, N.; Bock, A.; Dingermann, T.; Abdel-Tawab, M.; Schubert-Zsilavecz, M. Carnosic Acid and Carnosol, Phenolic Diterpene Compounds of the Labiate Herbs Rosemary and Sage, Are Activators of the Human Peroxisome Proliferator-Activated Receptor Gamma. *Planta Med.* **2006**, *72*, 881–887.

(47) Obach, R. S. Prediction of Human Clearance of Twenty-Nine Drugs from Hepatic Microsomal Intrinsic Clearance Data: An Examination of In Vitro Half-Life Approach and Nonspecific Binding to Microsomes. *Drug Metab. Dispos.* **1999**, *27*, 1350–1359.

(48) Brian Houston, J. Utility of in Vitro Drug Metabolism Data in Predicting in Vivo Metabolic Clearance. *Biochem. Pharmacol.* **1994**, *47*, 1469–1479.

(49) Zhang, W.; Lohman, A. W.; Zhuravlova, Y.; Lu, X.; Wiens, M. D.; Hoi, H.; Yaganoglu, S.; Mohr, M. A.; Kitova, E. N.; Klassen, J. S.; Pantazis, P.; Thompson, R. J.; Campbell, R. E. Optogenetic Control with a Photocleavable Protein, Phocl. *Nat. Methods* **2017**, *14*, 391–394.

(50) Da Costa, L. T.; Jen, J.; He, T. C.; Chan, T. A.; Kinzler, K. W.; Vogelstein, B. Converting Cancer Genes into Killer Genes. *Proc. Natl. Acad. Sci. U.S.A.* **1996**, *93*, 4192–4196.